Research Article ISSN 2766-2624

Advances in Earth and Environmental Science

Phosphorus Adsorption as Affected by Concretionary Nodules of Oxic Rhodustalf in Southern Guinea Savannah Agroecological Zone of Nigeria

David Emmanuel[1,3]; Adeyemo Adebayo Jonathan[1*]; Adejoro Solomon Alaba[1], Oluwagbemi Israel Adegbile[1]; Adebayo Mathew Ayorinde[2] and Ewulo Babatude Sunday[1]

[1]*Department of Crop, Soil and Pest Management, Federal University of Technology, Akure, Nigeria*

[2]*Department of Industrial Chemistry, Federal University of Technology, Akure, Nigeria.*

[3]*Agricultural and Rural Management Training Institute, Ilorin, Nigeria.*

***Corresponding author**

Adeyemo Adebayo Jonathan,
Department of Crop,
Soil and Pest Management,
Federal University of Technology,
Akure, Nigeria

Submitted : 1 Aug 2024 ; Published : 31 Aug 2024

Citation: David, E. et al., (2024). Phosphorus Adsorption as Affected by Concretionary Nodules of Oxic Rhodustalf in Southern Guinea Savannah Agroecological Zone of Nigeria. Adv Earth & Env Sci.; 5(3):1-15. DOI : https://doi.org/10.47485/2766-2624.1056

Abstract

Hard, rounded masses of mineral matter, known as concretionary nodules, can be found in soil or sedimentary rock. These nodules are typically made up of minerals like iron oxides, hydroxides, and carbonates that have been deposited in groundwater. Their sizes can range from small pebbles to large boulders, and they often differ in composition or hardness compared to the surrounding rock or soil. Nodules act as a highly effective storage space for extra P, leading to a significant increase in overall P requirements. Phosphorus, although an essential element for all living organisms, including plants and animals, is scarce. Despite its importance, only a small fraction of the total phosphorus available can be readily absorbed by plants. Given the worldwide demand for phosphorus in food production, it is crucial to devise techniques for extracting it from different sources. However, there has been limited research on the understanding of phosphorus availability and adsorption mechanisms in these areas. Therefore, the study focused on exploring the impact of concretionary nodules on phosphorus sorption and the characteristics of low-activity clay soil in the Guinea savannah of Nigeria. Soil samples collected from the study area were used to investigate the soil's ability to absorb phosphorus at depths ranging from 0 to 30-60-90-120-150 cm in different soil and concretion locations. Various soil and concretion types demonstrated distinct capacities for phosphorus adsorption, as indicated by the adsorption isotherm. The maximum monolayer adsorption capacities (Qmax values) were 161.0, 154.5, 149.6, 141.7, 139.8, and 139.3 mg/g for OBC, OBS, OC, OIS, OS, and OIC, respectively. At equilibrium with a 50-ppm solution, the pseudo-second-order rate constants for P sorption were 1.180 x 10^{-4}, 9.740 x 10^{-5}, 1.120 x 10^{-4}, 1.140 x 10^{-4}, 1.000 x 10^{-4}, and 8.010 x 10^{-5} g mg^{-1} min^{-1} for OIS, OIC, OBS, OBC, OS, and OC, in that order. In the 300-ppm equilibrium solution, the OIS, OIC, OBS, OBC, OS, and OC pseudo-second-order rate constants were 1.250 x 10^{-4}, 1.130 x 10^{-4}, 9.550 x 10^{-5}, 1.040 x 10^{-4}, 2.750 x 10^{-4}, and 1.420 x 10^{-4} g mg^{-1} min^{-1}, respectively. At the 500-ppm equilibrium, the pseudo-second-order rate constants for OIS, OIC, OBS, OBC, OS, and OC were 1.240 x 10^{-4}, 1.090 x 10^{-4}, 1.020 x 10^{-5}, 1.100 x 10^{-4}, 2.730 x 10^{-4}, and 1.180 x 10^{-4} g mg^{-1} min^{-1}, respectively. Consequently, the soil adsorption capacity increased with higher pseudo-second-order rate constants.

Keywords: Concretionary nodules, P-adsorption, Guinea Savannah, Kinetics, Equilibrium.

Introduction

The soils in the southern Guinea savannah of Nigeria are known to suffer from significant nutritional deficiencies and fertility limitations naturally (Adnan et al., 2017) These deficiencies are in part due to the low Organic Matter (OM) content (Johan et al., 2021) resulting from human activities, predominant vegetative cover, and local geology. Consequently, these factors impact the physical, chemical, and biological processes and kinetics that influence agricultural productivity and nutrient availability to plants (Asomaning et al., 2018; Sposito 2008). As the world's population is expected to hit 9.1 billion by 2050 (Fink et al., 2016) the existing food demand will need to increase twofold. Thus, any variations in nutrient deficiencies could result in economic harm, as seen in the growing food demand and fertilizer shortages globally (Cordell et al., 2009). This emphasizes the need to promote efficient nutrient utilization to meet the rising agricultural production requirements while ensuring environmental sustainability. Consequently, there is a growing focus on phosphorus as a finite resource due to the increasing need for agricultural production (Cordell et al., 2009).

Phosphorus is a crucial nutrient for agricultural and ecosystem productivity, serving as a limiting nutrient yet a finite resource (Nafiu, 2009) In areas where the soils are typically lacking

in P and abundant in iron and aluminium oxides, referred to as "kaolinitic soils" with low clay contents, P availability is negatively influenced (Samad, 2006). The limited availability of phosphorus in these soils is due to its slow diffusion and strong fixation. Hence, maintaining an ideal phosphorus supply in the root zone can boost the capacity of plant roots to mobilize and absorb phosphorus from the rhizosphere. These soils are further identified as a type of kaolinitic clay, which is a 1:1 clay mineral. Studies have shown that kaolinitic clay retains phosphorus (P) more effectively compared to 2:1 clay mineral (de Campos et al., 2016; Hooda et al., 2000). Phosphorus adsorption plays a significant role in the movement of phosphorus from soil to water, affecting its availability and distribution (Moody, 2011; Abdu & Etiene 2015). The diffusion of phosphorus into the root system is mainly controlled by soil water content, diffusion coefficient, and soil buffer power, which are crucial factors affecting the P diffusion to plant roots.

In the Nigerian savannah, soils are marked by low phosphorus (P) content and high phosphorus sorption (Hooda et al., 2000; Agbenin, 2003; Zhang et al., 2014). The presence of iron (Fe) and aluminum (Al) oxides, hydroxides, and oxi-hydroxides in these soils result in a strong affinity for phosphorus, leading to considerable phosphorus fixation (Asomaning et al., 2018; Nafiu, 2009; Abdu & Etiene 2015; Agbenin, 2003). This is due to the pH-dependent surface charge of these oxides. Often found as concretionary nodules in highly weathered tropical soils, these nodules have higher phosphorus content than the surrounding soil, thus retaining phosphorus in a less soluble form (Zhang et al., 2014). According to (Fink et al., 2016). these concretions serve as phosphorus reservoirs. At the same time, contain significant iron and aluminum oxide content, which effectively captures additional phosphorus, as noted by (Wang et al., 2013). For instance, concretionary soils such as lateritic ferruginous nodules are recognized for their ability to absorb substantial quantities of phosphate. Ferruginous nodules, commonly found in concretionary soils, often have higher P content compared to the neighboring soils, making them efficient traps for additional soluble P, as indicated by (Fink et al.,2016), and (Zhang et al., 2014). The soils possess a strong ability to retain additional P due to their high reactivity, allowing for P fixation through sorption. The presence, distribution, and abundance of these nodules or concretions significantly affect the soil's nutrient status and phosphate availability (Agbenin, 2003; Bortoluzz, 2015). Despite the extensive weathering and high levels of free iron (Fe) oxides in savannah soils, their phosphorus sorption capacity is relatively low (Nafiu, 2009). Savannah soils also consist of variable charge minerals, leading to P unavailability to plants due to the prevalence of sesquioxide and low-activity clay content, particularly in Oxisols, Ultisols, and Alfisols.

To avoid future food crises in West Africa, it is essential to tackle the issues of P deficiency and availability, particularly in intensive land use systems, along with addressing other nutrient deficiencies. Research on the concretionary components of southern Guinea savannah soils is still incomplete, and more investigation is needed to determine their potential for retaining nutrients, especially in terms of phosphate sorption. Due to demographic pressures, there has been an increase in land use intensity and cultivation of marginal lands, resulting in low productivity despite the use of inorganic P fertilizer. Often, the restricted availability of P is the main factor limiting soil productivity. Consequently, this study seeks to fill the knowledge gap regarding the influence of concretionary nodules on the adsorption of soil P (both organic and inorganic) in the Nigerian Southern Guinea Savannah Region.

Materials & Methods

A brief description of the Study Area

The research included the collection of soil samples using soil sampling equipment from various areas across the Southern Guinean savannah. Specifically, the samples were obtained from three (3) communities in Kwara State, which are Owu Isin (latitude $08^0$16.58''N: longitude 05^o 55′6′′E), Obbo-Ile (latitude 08^0 77′.5′′N: longitude 05^o. 18′ 7′′E), and Osi (latitude 7^0 3′6′′N: longitude $5^0$08"7'E). These areas under study are situated within the Southern Guinea savannah ecology of Nigeria.

Climate of the Study Area

The areas under study experience a bimodal rainfall pattern, receiving around 1600 mm of rainfall with two peaks in July and September, and a dry period in August. The mean daily maximum temperature in the study areas ranges from 28 °C to 34 °C, while the mean daily minimum temperature varies from 24 °C to 26 °C. During the day, the relative humidity ranges from 75 %, while at night, it reaches 96 %.

Land Use of the Study Areas

The study areas primarily involve arable and livestock farming as the major types of land use. Subsistence farming, which involves intensive and continuous cultivation, is prevalent in arable farming. The area primarily cultivates sorghum, maize, cowpea, groundnuts, soybeans, and vegetables as the main crops.

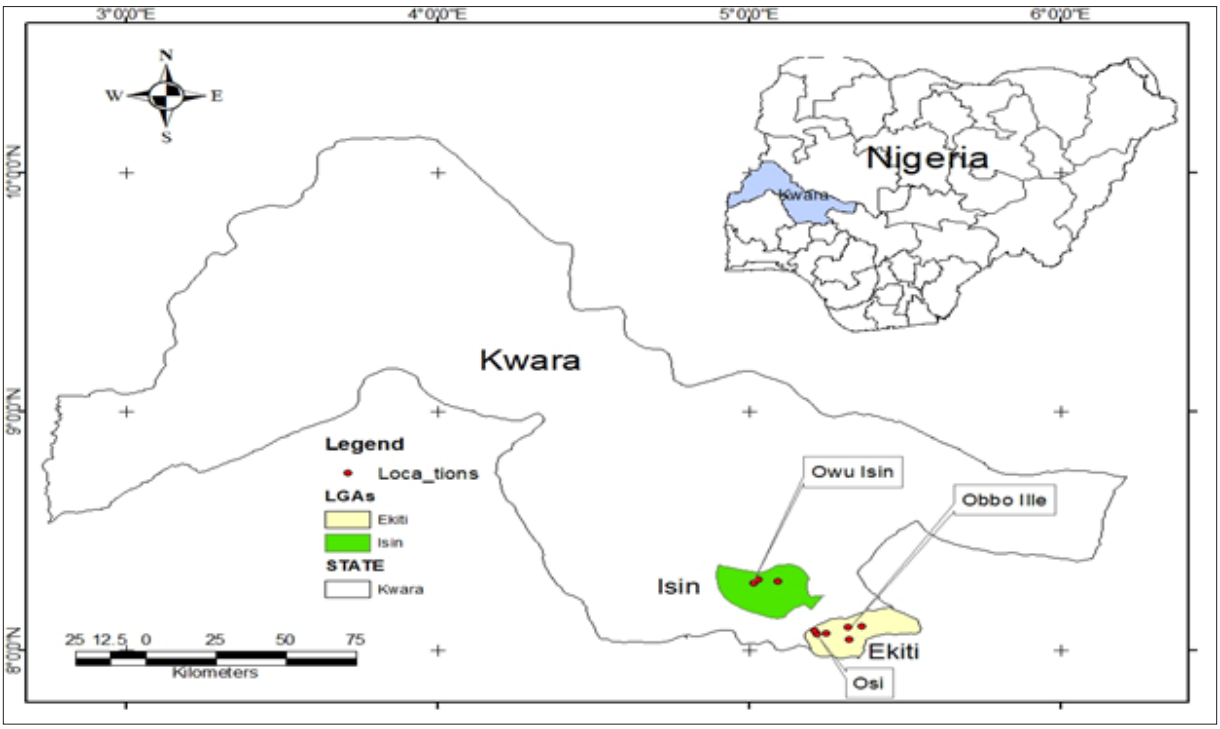

Map of the Study Area

Soil Mineralogy of the Study Areas

The study areas are characterized by crystalline Precambrian basement complex rocks, which include both metamorphic and igneous formations, as well as sedimentary rock (Oriola et al., 2019). In some parts, there are significant deposits of ferruginous tropical soils overlying these crystalline acid rocks. The region features highly weathered red and yellowish-brown ferralsols in certain locations. The soil is classified as moderately deep, reddish, sandy clay loam with plinthite at depth, well-drained, and categorized as Ferric Luvisol (FAO, 1988) and Oxic Rhodustalf (USDA, 1975). Overall, the soil is a leached tropical ferruginous type situated on a deeply weathered Precambrian basement complex, with ironstone gravels and ferruginized sandstone being prevalent at higher elevations, contributing to the formation of well-drained soils.

Soil Sampling Method

The study utilized soil samples gathered from three communities as mentioned earlier. These communities were chosen based on previous reports from farmers regarding the ineffectiveness of fertilizer application on the soils. Within each community, farms displaying visible concretionary nodules were located. Soil profiles were excavated on these identified farms, and samples were obtained from various depths within the profiles. The collected soil samples ranged from depths of 0-30 cm, 31-60 cm, 61-90 cm, 91-120 cm, and 121-150 cm. Each profile was marked with soil horizon boundaries, and the depth of each designated horizon was measured. Laboratory analyses were conducted on soil samples collected from each genetic horizon, with three replicates taken. The samples were air-dried, sieved, and stored for subsequent analysis of soil nutrients and texture.

Separation of Concretionary Nodules

The collected soil samples were air-dried and then sieved through a 2-mm mesh to remove concretionary nodules while retaining stones and gravel. The nodules were subsequently ground to pass through the same 2-mm sieve and stored in plastic cups for future analysis. The fine soil fractions were also ground to pass through a 2-mm sieve and stored in plastic cups for subsequent nutrient analysis.

Laboratory Analyses

To assess the physical and chemical properties of concretionary nodules and fine soils, internationally approved techniques were employed. These analyses covered particle size distribution, soil pH, organic carbon (OC), exchangeable bases (Ca^{2+}, Mg^{2+}, K^{+}, and Na^{+}), available phosphorus, cation exchange capacity (CEC), and included studies on phosphorus adsorption, desorption, and kinetics.

Phosphorus adsorption study on soil and concretions

Phosphorus adsorption was investigated using three sample types: bulk soil with concretions, sieved soil without concretions, and concretions alone. Duplicate 2-gram samples of each were weighed and placed into 50 ml centrifuge tubes. These samples were mixed with orthophosphate solutions at various concentrations (0, 50, 100, 250, 500, and 1000 µg P/g soil) in a 0.01 M KCl solution. To maintain a soil-to-solution ratio of 1:10, the tubes were filled to the 20 mL mark with KCl solution. The mixtures were shaken for two hours on a reciprocating mechanical shaker, and then filtered through Whatman No. 42 filter paper. Phosphorus content in the filtered solution was measured using the Murphy and Riley (Murphy et al., 1962). method. Phosphorus adsorption was determined by comparing the initial phosphorus concentration with the amount remaining in the solution.

Adsorption Isotherm and Kinetic Models

The phosphorus adsorption data was analyzed using both the Langmuir and Freundlich adsorption isotherm models.

Langmuir equation is expressed as:

$$\frac{C}{q} = \frac{1}{kb} + \frac{C}{b}$$

Where

q = the amount of P adsorbed per unit weight of soil (mg kg^{-1}),
c = equilibrium P concentration (mg kg^{-1}),
b = P adsorption maxima (mg kg^{-1}),
k = coefficient relating to bonding energy (mg kg^{-1}) and
kb = distribution coefficient (mg kg^{-1}).

The Freundlich equation is given by

$q=Kf\ C_q^{1/n}$

Where;

KF and n are the Freundlich constants characteristic of the system involved;

KF and n are indicators of adsorption capacity and adsorption intensity, respectively.

KF and n can easily be determined from the linearized logarithmic form of the equation given by:

Log q = log KF + 1/n log Cq

The equilibrium (concentration-dependent) data were subjected to non-linear Langmuir and Freundlich models, which as are shown in Equations 1 and 2, respectively.

$$Q_e = \frac{Q_{max} \cdot K_L \cdot C_e}{1 + K_L \cdot C_e} \quad (1)$$

$$Q_e = K_L \cdot C_e^{\frac{1}{nF}} \quad (2)$$

where Q_e = amount of phosphate adsorbed by soils and concretions at equilibrium (mg/g); Q_{max} = maximum adsorption capacity of the soil and concretion types (mg/g), C_e = equilibrium concentration of the adsorbate (mg/L), K_L = Langmuir equilibrium constant (L/mg), K_F = Freundlich equilibrium constant $\left\{(mg/g)(mg/L)^{-\frac{1}{nF}}\right\}$, and *nF* = dimensionless exponent of the Freundlich model.

The time-dependent kinetic data were analyzed using non-linear pseudo-first order, pseudo-second order, and Elovich chemisorption models, with their respective mathematical representations provided in Equations 3 to 5.

$$Q_t = Q_e\left[1 - e^{(-k_f \cdot t)}\right] \quad (3)$$

$$Q_t = Q_e - \frac{Q_e}{1 + (k_s \cdot Q_e \cdot t)} \quad (4)$$

$$\frac{dQ_t}{dt} = \alpha \cdot e^{(-\beta \cdot Q_t)} \quad (5)$$

where Q_t = amount of phosphate adsorbed by soils and concretions (mg/g) at a time, *t;* k_f = pseudo-first-order rate constant (min^{-1}), k_s = pseudo-second-order rate constant (g/mg min), α = initial adsorption rate (mg/g min), and β = parameter that describes the surface coverage and the activation energy of the chemisorption (g/mg).

The kinetic studies were carried out using three different concentrations (50, 300, and 500 mg/L) of phosphate to unravel the details kinetic characteristics of the soil and concretion types.

The judgement of model fitness was done using correlation coefficient ($R^{2)}$ and standard deviation (SD), which are presented in Equations 6 and 7, respectively.

$$R^2 = \frac{\sum_i^{n_p}(Q_{i,expt} - \bar{Q}_{expt})^2 - \sum_i^{n_p}(Q_{i,expt} - \bar{Q}_{i,model})^2}{\sum_i^{n_p}(Q_{i,expt} - \bar{Q}_{expt})^2} \quad (6)$$

$$SD = \sqrt{\frac{1}{n-p} \cdot \sum_i^{n}(Q_{i,expt} - Q_{i,model})^2} \quad (7)$$

where Q_i, model = each value of Q predicted by the fitting model, $Q_{i,expt}$ = each value of Q measured experimentally, = average of Q measured experimentally, n_p = number of experiments performed, and p = number of parameters of the fitting model.

Recovery of adsorbed phosphate on soils and concretions

Phosphate recovery was evaluated from both sieved soils without concretions and the concretions separately. Ten grams of each soil sample were weighed into plastic vials, and 100 µg of KH_2PO_4 in 0.1 M KCl was added. The suspensions were allowed to equilibrate for 72 hours at field capacity, which was determined gravimetrically. Afterward, the phosphorus-saturated soil was air-dried and sieved through a 2-mm mesh. Subsequently, 1 gram of the air-dried soil sample was placed into a centrifuge tube, and phosphorus was extracted using a Bray-1 solution. The extraction process involved shaking for 5, 10, 30, 60, 120, 240 minutes, and 16 hours.

Owu Isin Soils = OIS
Owu Isin Concretions = OIC
Obbo-Ile Soils = OBS
Obbo-Ile Concretions = OBC
Osi Soils = OS
Osi Concretions = OC

Statistical Analysis

The analysis of variance (ANOVA) was used to identify significant differences in phosphorus dynamics among bulk soil with concretions, sieved soil without concretions, and the concretions alone. Statistical analyses were performed using (Excel, 2007).and SAS Statistical Software version 9 (2002).

Result

Affinity of Soil and Concretion Samples with Phosphorus

The study examined the adsorption mechanisms onto soil samples using the Langmuir and Freundlich isotherm models. Figures 1-6 illustrate the equilibrium profiles of these models, and the parameters are summarized in Table 1. Langmuir's model assumes that adsorbate forms a monolayer on the adsorbent, while Freundlich's model allows for multilayer adsorption. The SD values in Table 1 indicate that the Langmuir

model most effectively describes phosphorus adsorption onto the soil samples. This model gave the lowest SD values and highest values. Going by the Langmuir parameters in Table 1, the best soil type for phosphorus adsorption follows the trend OBC > OBS > OC > OIS > OS > OIC while OIC exhibited the lowest adsorption capacity for phosphorus. The maximum monolayer adsorption capacities (Qmax values) are 161.0, 154.5, 149.6, 141.7, 139.8, and 139.3 mg/g for OBC, OBS, OC, OIS, OS, and OIC, respectively. The high adsorption capacity of phosphorus could be attributed to the high porosity of OBC could be responsible for the high adsorption capacity of phosphorus.

Equilibrium study of Phosphorus Adsorption onto Owu Isin, Obo Ile, and Osi under Soils and concretions

The Langmuir adsorption model (figure 1) revealed that OIS had an adsorption capacity of 141.7 mg/g under the specified conditions, with comparisons made to other soil orders and concretion types. This outcome could be attributed to the soil's low porosity, which is not conducive to adsorption. Additionally, the high available phosphorus content in this sample may also have played a role. Similarly, Figure 2 depicts the adsorption capacity of OIC (139.3 mg/g) under the same conditions using the Langmuir adsorption model, comparing it to other soil orders and concretion types. This value indicates the lowest adsorption rate among the samples evaluated, likely due to the low porosity of the soil, which is not favourable for adsorption. The high phosphorus content available in this sample could also play a role. The Owu Isin concretion (OIC) demonstrates good agreement with the Langmuir model, as evidenced by a regression coefficient of 0.9940, which is near 1. Furthermore, the adsorption capacity of OS is 149.6 mg/g, ranking it as the third highest value under the specified conditions using the Langmuir adsorption model in comparison to other soil and concretion types. It also shows strong compliance with the Langmuir model at a rate of 0.9943. Furthermore, the adsorption capacity of OBS is 154.5 mg/g (figure 4), making it the second highest value under the Langmuir adsorption model compared to other soil orders and concretion types under similar conditions. The Langmuir model is well-suited for Obbo Ile soil (OBS), as evidenced by the high regression coefficient value of 0.9959, which indicates strong conformity. The high adsorption capacity of OBS may be attributed to its amorphous iron and low available phosphorus content, which significantly bolster the adsorption process.

In addition, the sorption data of Obbo Ile concretion (OBC) demonstrates strong adherence to the Langmuir adsorption isotherm, as depicted in Figure 1, with a regression coefficient value of 0.9972, a figure remarkably close to 1 when compared to other soil orders and concretion types in similar conditions. Additionally, OBC exhibited the highest adsorption capacity of 161.0 mg/g, as shown in Figure 1. The high adsorption capacity might result from the presence of amorphous iron and low available phosphorus content, both of which significantly boost adsorption. The Langmuir model is identified as the most suitable isotherm model for describing phosphorus adsorption onto the soil and concretion samples, as evidenced by its lowest standard deviation (SD) and highest correlation values. As per the Langmuir parameters listed in Table 1, the order of soil types based on phosphorus adsorption capacity is OBC > OBS > OC > OIS > OS > OIC, with OIC demonstrating the lowest adsorption capacity. The maximum monolayer adsorption capacities (Qmax values) are 161.0, 154.5, 149.6, 141.7, 139.8, and 139.3 mg/g for OBC, OBS, OC, OIS, OS, and OIC, respectively. The high porosity of OBC may be accountable for its high capacity to adsorb phosphorus. In terms of the absorption of phosphate by soil and concretion samples at various depths depicted in Figure 2, the adsorption rate rises with increasing concentration, suggesting that the adsorbent has more active sites for a relatively high phosphate concentration. For example, at depths of 30-60, 60-90, and 90-120 cm (refer to Figure 2), OIS displayed the highest adsorption at a very high phosphate concentration, with a higher concentration of phosphate leading to a proportional increase in the amount of adsorbed phosphate. This pattern was observed across all depths and samples examined, with the lowest value recorded in the OIS at a depth of 15-30 cm. The highest adsorption at a very high phosphate concentration was observed at 0-15 cm depth for OIC, as shown in Figure 2. With increasing phosphate concentration, there was a corresponding increase in phosphate adsorption for OIC, and the lowest value was found at a depth of 0-15 cm. OBS showed the highest adsorption at very high phosphate concentrations across all depths, as seen in Figure 2. As phosphate concentration increased, the amount of phosphate adsorbed similarly increased, with the lowest adsorption values found at depths of 30-60 cm and 60-90 cm for OBS, respectively. Observations for OBC (Figure 2) indicated that it exhibited the highest adsorption at a very high phosphate concentration at depths of 30-60 cm, 60-90 cm, and 90-120 cm. The increase in phosphate concentration led to higher phosphate adsorption, and the OBC at a depth of 0-15 cm showed the lowest recorded value. At a very high phosphate concentration, the Osi soil (OS) at a depth of 90-120 cm demonstrated the highest adsorption. As the phosphate concentration increased, the amount of phosphate adsorbed also increased, with the lowest value observed in the OS at a depth of 0-15 cm (refer to Figure 2). Lastly, the OC at a depth of 30-60 cm exhibited the highest adsorption at a very high phosphate concentration, as depicted in Figure 2. The increase in phosphate concentration resulted in a higher quantity of phosphate adsorbed, with the lowest value recorded in the OC at a depth of 30-60 cm.

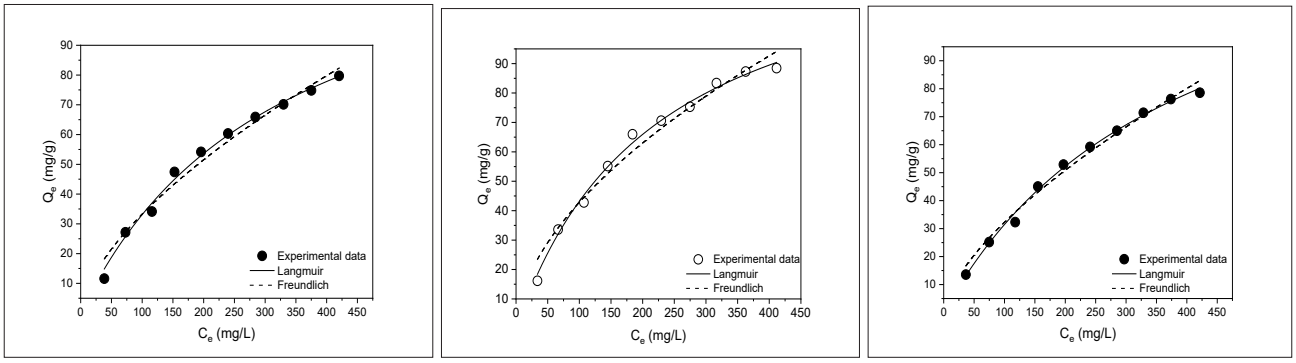

(OIS) (OIC) (OBS)

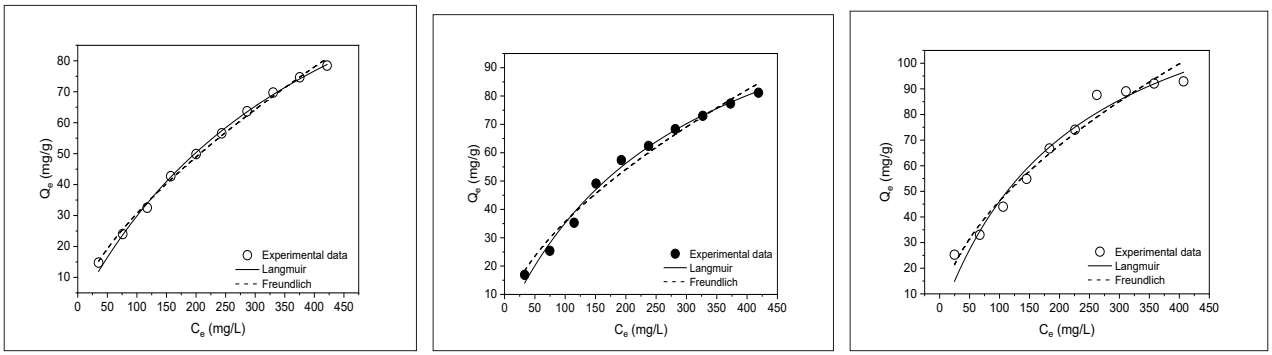

(OBC) (OS) (OC)

Figure 1: Equilibrium modelling of phosphorus adsorption under different locations and farmer's field.

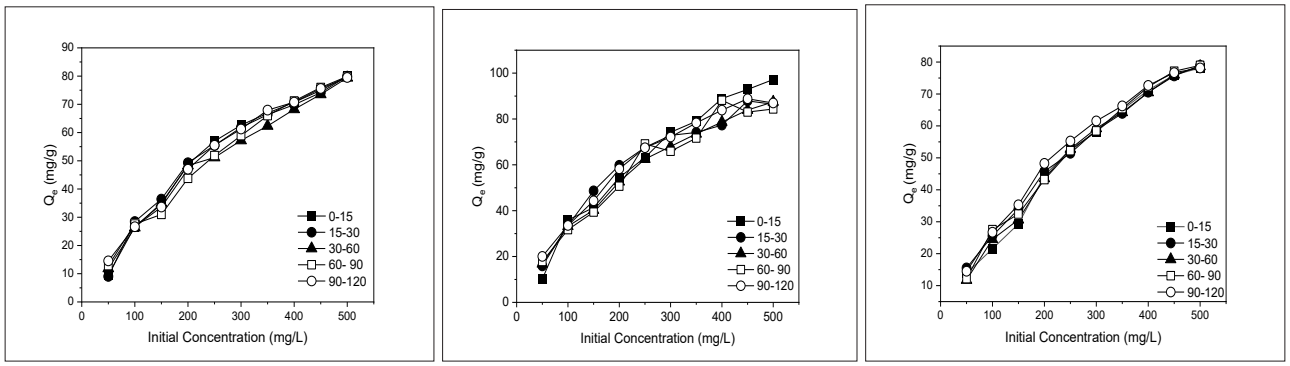

(OIS) (OIC) (OBS)

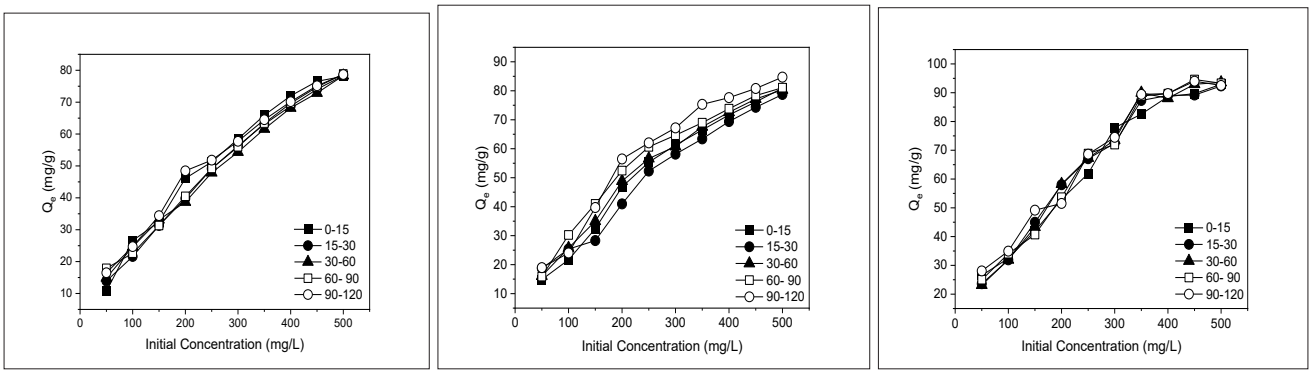

(OBC) (OS) (OC)

Figure 2: Effect of initial concentration of phosphate on the amount of phosphate removed by different locations and farmer's field.

Time study of Phosphorus Adsorption at different concentrations onto Owu Isin, Obo Ile, and Osi under Soils and concretions

Figure 3 illustrates the influence of time on the adsorption of 50 ppm phosphate. There was a corresponding increase in adsorption as time elapsed. Specifically, a substantial rise in adsorption was noted between 0 and 350 minutes. For example, OIS displayed the highest adsorption at 350 minutes but the lowest at 90-120 cm depth, under 50 minutes (Figure 3). In contrast, OIC demonstrated the lowest adsorption in the initial 50 minutes (refer to Figure 3), with a gradual increase until one hour later, followed by intermittent upward movements, and its peak was observed at a depth of 15-30 cm. Similarly, as depicted in Figure 3, there was a noticeable uptick in adsorption over time for OBS, with the lowest adsorption occurring at a depth of 15-30 cm and the highest at 60-90 cm. In line with this pattern, OBC experienced a rise in adsorption until it peaked after 5 hours, starting from a minimal level at 30 minutes and reaching its nadir at a depth of 0-15 cm (Figure 3). Figure 3 illustrates that OS had the lowest adsorption at a depth of 30-60 cm and steadily increased, reaching its highest point at 350 min. Osi concretion (OC) demonstrated the lowest adsorption values at depths of 60-90 cm, also achieving the highest at a depth of 90-120 cm from 300 min and onwards (Figure 3).

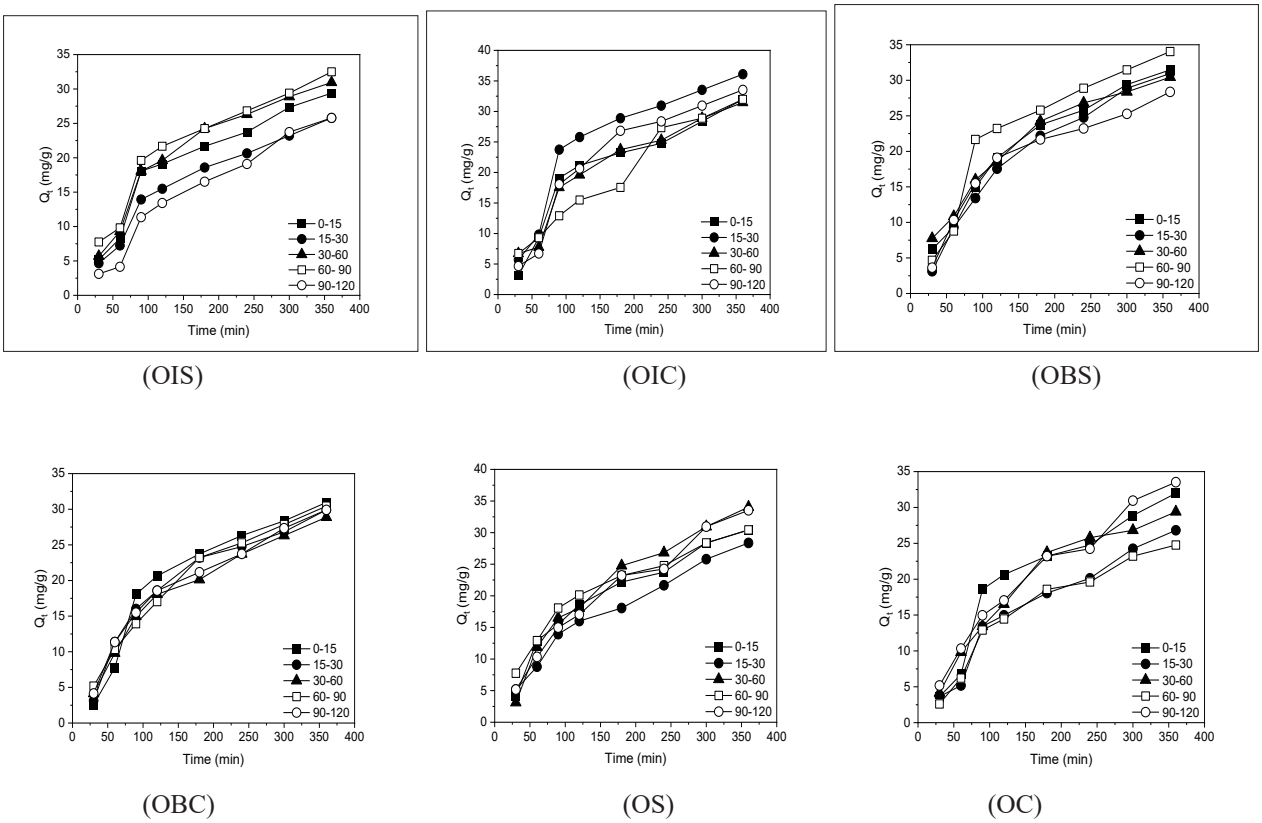

Figure 3: Effect of time on the adsorption of phosphate by different locations and farmer's field at 50 ppm

The effect of time on the adsorption of phosphate at 300 ppm concentration is illustrated in Figure 4. Adsorption increased as time advanced. There was a significant rise in adsorption between 0 and 350 minutes. OIS achieved the highest adsorption at a depth of 30-60-90 cm after 350 minutes, while the lowest was below 50 minutes at 15-30 cm (Figure 4). In contrast, for OIC, the lowest adsorption occurred at 15-30 cm below 50 minutes, with a slight increase observed within the next hour, followed by sporadic ups and downs, and its peak was observed at the same depth of 15-30 cm (Figure 4). Similarly, there was a notable uptick in adsorption over time for OBS (refer to Figure 4), with the least adsorption occurring at a depth of 90-120 cm and the most at 60-90 cm. OBC displayed the highest adsorption at 60-90 cm after 350 minutes, but lower values across all depths, with the least at a depth of 30-60 cm (Figure 4). As depicted in Figure 4, OS showed a minimal increase in adsorption from 30 minutes to an hour, with the lowest value recorded at a depth of 30-60 cm. Nevertheless, all depths followed a similar pattern before diverging after 100 minutes, reaching its peak at 90-120 cm after 300 minutes. In Figure 4, the adsorption of phosphate in OC displayed interesting trends. Lower rates were observed at depths of 0-15 cm during the initial time frame, but there were noticeable changes with increasing time, leading to peak adsorption at 0-15 cm.

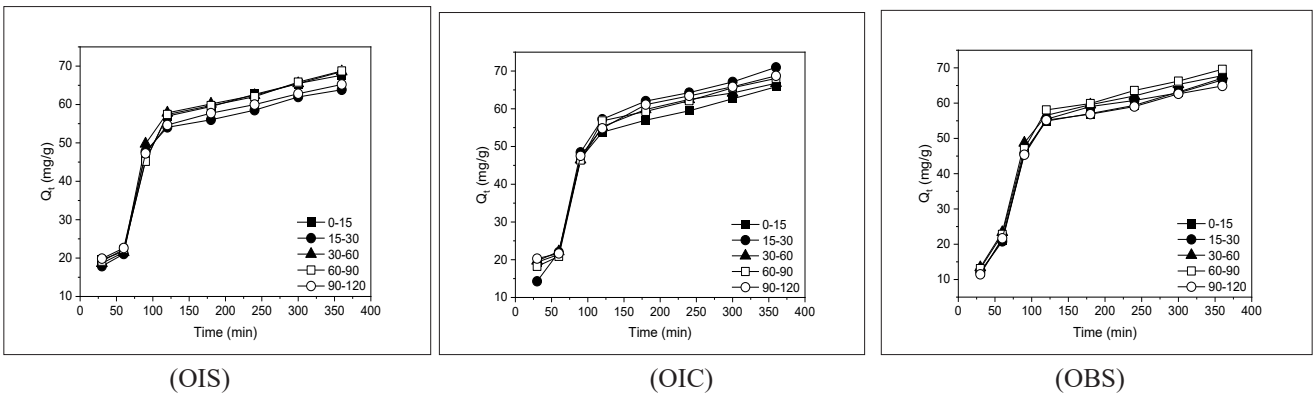

(OIS) (OIC) (OBS)

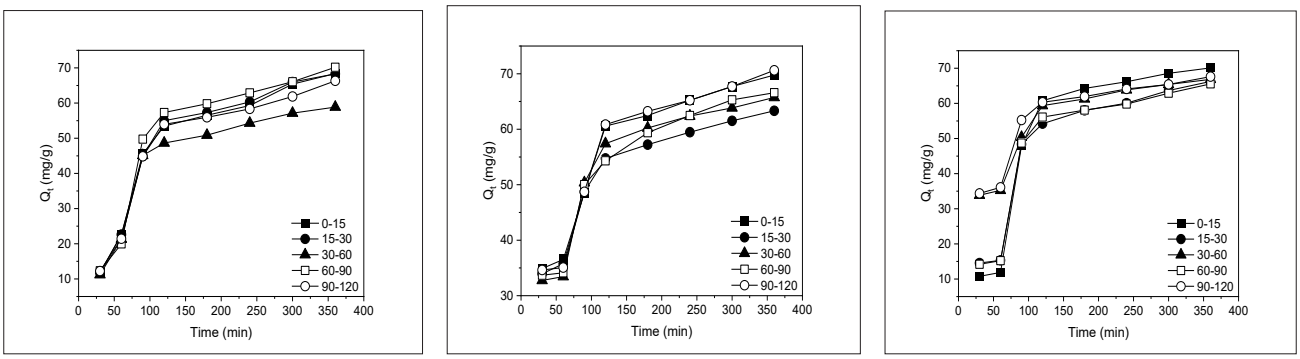

(OBC) (OS) (OC)

Figure 4: Effect of time on the adsorption of phosphate by different locations and farmer's field at 300 ppm

Figure 5 depicts the impact of time on phosphate adsorption at 500 ppm concentration. Adsorption increased proportionally with time, notably between 0 and 350 minutes. For example, OIS exhibited higher adsorption at 350 minutes at depths of 0-15-30-60-90 cm, but the lowest at 90-120 cm, within 50 minutes (refer to figure 5). Furthermore, as depicted in Figure 5 the minimal adsorption for OIC was observed at a depth of 15-30 cm in less than 50 minutes, with a slight increase seen up to 1 hour later, and then a sporadic uptrend followed by a plateau. Nevertheless, the highest rates were noted at the same depth of 15-30 cm. Similarly, OBS exhibited lower adsorption at all depths (figure 5), followed by a rising trend that levelled off after 100 minutes, reaching peak values at 30-60 cm and 60-90 cm, respectively. A parallel pattern was evident in OBC across depths. However, it indicated the lowest adsorption rates at a depth of 60-90 cm and relatively higher rates across all depths except at 30-60 cm, reaching peak values at 60-90 cm (Figure 5). Additionally, there was an upward trend in OS from 30 to 120 minutes, followed by a period of stability. The peak of OS was reached at 90-120 cm after 350 minutes. The absorption of phosphate in OC exhibited intriguing patterns, with the 0-15 cm depth showing the lowest rates at shorter time intervals but displaying significant changes as time progressed. After 120 minutes, most depths showed a seemingly consistent stable trend, with the peak being reached at depths of 90-120 cm (Figure 5).

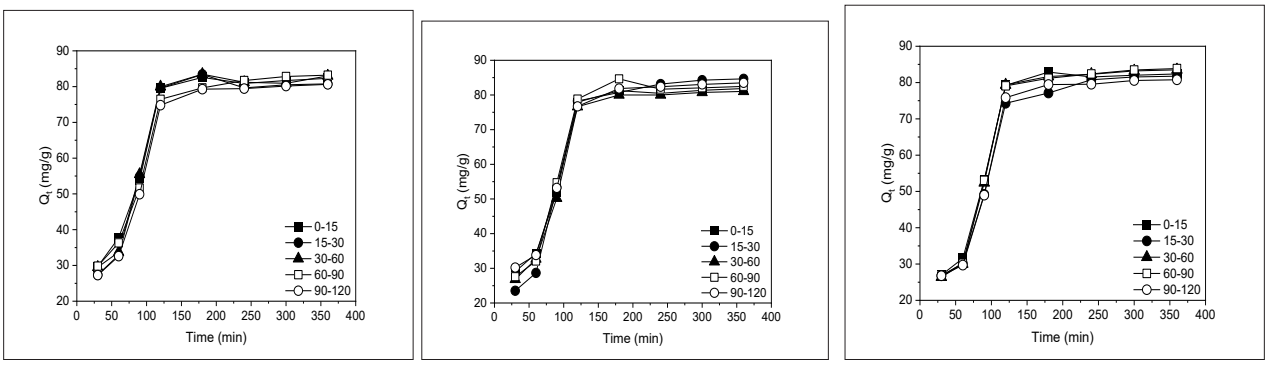

(OIS) (OIC) (OBS)

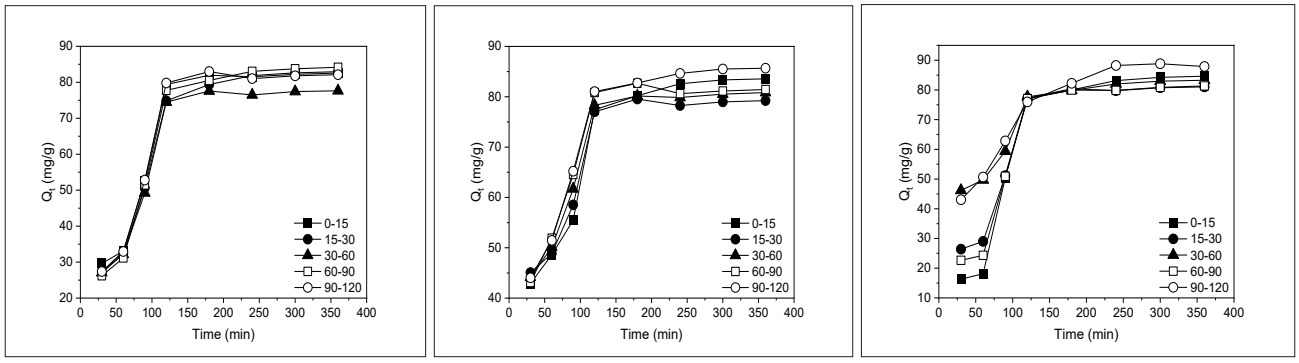

(OBC) (OS) (OC)

Figure 5: Effect of time on the adsorption of phosphate by different locations and farmer's field at 500 ppm

Kinetics Modelling of Adsorption of Phosphorus onto Owu Isin, Obo Ile, and Osi under Soils and Concretions

The time-dependent data were analyzed using pseudo-first-order and pseudo-second-order kinetic models. The kinetic profiles of OIS, OIC, OBS, OBC, OS, and OC are summarized in Table 1. According to the SD values, the pseudo-second-order model is a better fit for phosphorus adsorption onto all soil samples than the pseudo-first-order model. The pseudo-second-order model provided higher R^2 values and lower SD values than the pseudo-first-order model. Furthermore, the pseudo-second-order equilibrium adsorption capacities (Qe (model)) for all soil samples are more accurate than the Qe (expt). The pseudo-second-order rate constants are as follows: 3.050 x 10^{-3}, 4.500 x 10^{-3}, 2.560 x 10^{-3}, 2.280 x 10^{-3}, 3.370 x 10^{-3}, and 4.460 x 10^{-5} g $mg^{-1}min^{-1}$for OIS, OIC, OBS, OBC, OS, and OC, respectively. The rate constant is directly proportional to the rate of reaction. According to the rate constants, the order of decreasing phosphorus adsorption rate by soil samples is OBC > OBS > OIS > OS > OC > OIC. The rate of phosphorus adsorption by OBC was 1.4 times higher than that of OS. Furthermore, OBC adsorbed phosphorus twice as fast as both OIC and OC.

Model	Parameters	Owu Isin Soils	Owu Isin Concretions	Obbo-Ile Soils	Obbo-Ile Concretions	Osi Soils	Osi Concretions
Langmuir	Q_{max} (mg/g)	141.7	139.3	154.5	161.0	139.8	149.6
	K_L (L/mg)	3.050 x 10^{-3}	4.500 x 10^{-3}	2.560 x 10^{-3}	2.280 x 10^{-3}	3.370 x 10^{-3}	4.460 x 10^{-3}
	R^2	0.9933	0.9940	0.9959	0.9972	0.9912	0.9943
	SD	1.937	2.004	1.528	1.234	2.221	2.097
Freundlich	KF $\left\{(mg/g)(mg/L)^{-\frac{1}{nF}}\right\}$	0.4441	3.309	1.577	0.1525	2.221	3.602
	nF	0.1099	1.798	1.525	0.04358	1.659	1.804
	R^2	0.9785	0.9741	0.9942	0.99613	0.9805	0.9880
	SD	3.465	4.179	1.825	1.443	3.311	2.438

Table 1: Equilibrium parameters of soils and concretions

At a phosphate concentration of 50 mg/L, the time-dependent data were analyzed using pseudo-first-order, pseudo-second-order, and Elovich chemisorption kinetic models. Table 2 provides the kinetic profiles for OIS, OIC, OBS, OBC, OS, and OC, along with a summary of the study's parameters. Graphical representations are shown in Figure 6. The SD values in the table suggest that the pseudo-second-order model is the most suitable for describing phosphorus adsorption onto all soil samples, as it exhibits higher R^2 values and lower SD values compared to the pseudo-first-order and Elovich chemisorption models.

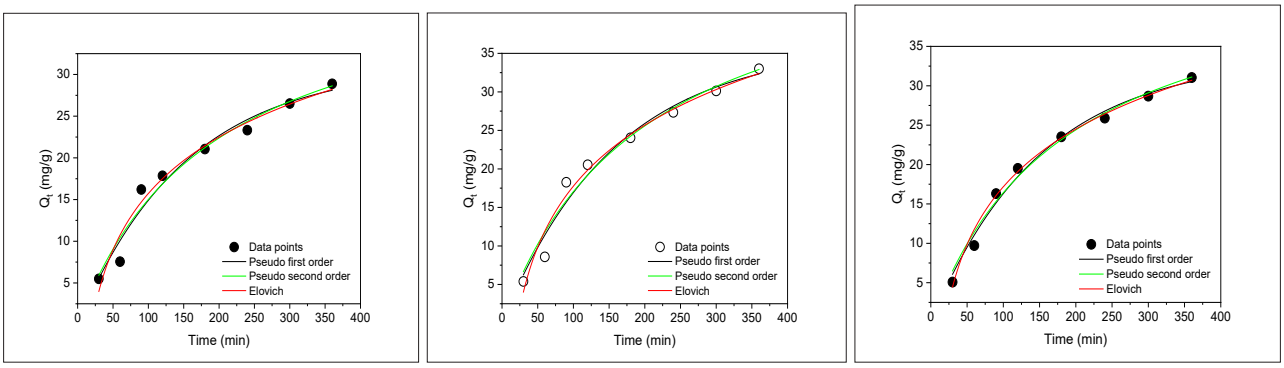

(OIS) (OIC) (OBS)

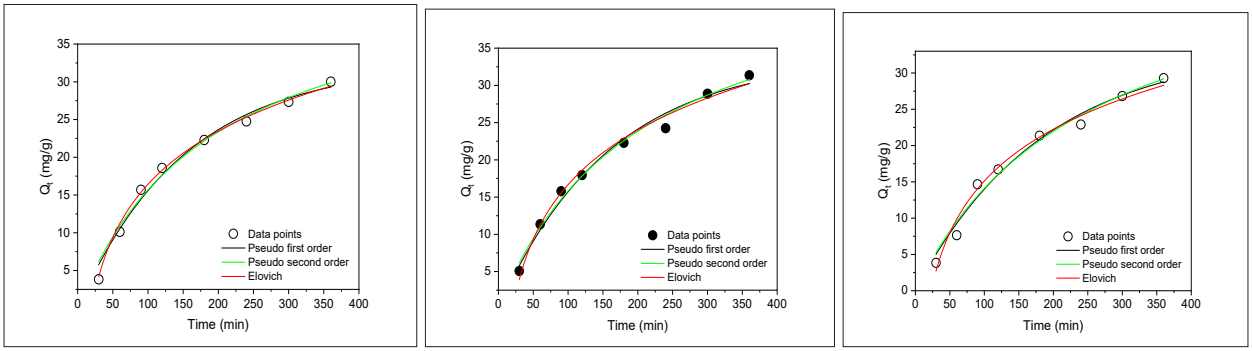

(OBC) (OS) (OC)

Figure 6: Kinetic modelling of adsorption of phosphate by different locations and farmer's field at 50 ppm

Models	Parameters	Owu Isin Soils	Owu Isin Concretions	Obbo-Ile Soils	Obbo-Ile Concretions	Osi Soils	Osi Concretions
Pseudo first order	$Q_{e(expt)}$ (mg/g)	28.88	33.01	31.05	30.02	31.36	29.30
	$Q_{e(model)}$ (mg/g)	31.06	2.709	33.60	32.33	1.856	33.61
	kF (min^{-1})	6.540×10^{-3}	1.030×10^{-3}	6.650×10^{-3}	6.570×10^{-3}	7.300×10^{-4}	5.390×10^{-3}
	R^2	0.9688	0.9723	0.9890	0.9856	0.9848	0.9816
	SD	1.607	1.774	1.037	1.154	1.181	1.312
Pseudo second order	$Qe_{(model)}$ (mg/g)	43.99	51.22	47.42	45.75	48.36	49.59
	kS (g/mg min)	1.180×10^{-4}	9.740×10^{-5}	1.120×10^{-4}	1.140×10^{-4}	1.000×10^{-4}	8.010×10^{-5}
	R^2	0.9985	0.9986	0.9984	0.9985	0.9987	0.9993
	SD	0.2436	0.2688	0.2714	0.2560	0.2442	0.1829
Elovich chemisorption	β (g/mg)	0.4893	0.04124	0.5374	0.5118	0.5114	0.4471
	α (mg/g min)	0.1026	0.005790	0.09474	0.09850	0.09452	0.09716
	R^2	0.9947	0.9747	0.9951	0.9948	0.9936	0.9895
	SD	0.5048	1.697	0.5269	0.5198	0.6025	0.7541

Table 2: Kinetic parameter of the adsorption of phosphate onto soils and concretions at 50 mg/L of phosphate

The accuracy of pseudo-second-order equilibrium adsorption predictions (Qe (model)) surpassed that of pseudo-first-order predictions in terms of Qe (expt)) for all soil samples. The pseudo-second-order rate constants are as follows: 1.180×10^{-4}, 9.740×10^{-5}, 1.120×10^{-4}, 1.140×10^{-4}, 1.000×10^{-4}, and 8.010×10^{-5} g mg^{-1} min^{-1} for OIS, OIC, OBS, OBC, OS, and OC, respectively. An increase in the rate constant corresponds to an increase in the rate of reaction. The rate of phosphorus adsorption by soil samples decreases in the order: of OS > OBS > OBC > OIS > OC > OIC based on the rate constant values. OS exhibited 8-9 times the rate of phosphorus adsorption compared to OBS, and OS adsorbed phosphorus over 8 times faster than both OIC and OC.

When the phosphate concentration was 300 mg/L, the time-dependent data were analyzed using pseudo-first-order, pseudo-second-order, and Elovich chemisorption kinetic models. The kinetic profiles and parameter summaries for OIS, OIC, OBS, OBC, OS, and OC are detailed in Table 3, with graphical illustrations in Figure 7. The SD values in Table 3 suggest that the pseudo-second-order model is the most effective at describing phosphorus adsorption on all soil samples, outperforming both the pseudo-first-order and Elovich chemisorption models in terms of R^2 and SD values. Furthermore, the pseudo-second-order model provided more accurate equilibrium adsorption capacities (Qe (model)) compared to the pseudo-first-order predictions. The pseudo-second-order rate constants are 1.250×10^{-4}, 1.130×10^{-4}, 9.550×10^{-5}, 1.040×10^{-4}, 2.750×10^{-4}, and 1.420×10^{-4} g mg^{-1} min^{-1} for OIS, OIC, OBS, OBC, OS, and OC, respectively. The order of decreasing phosphorus adsorption rate by soil samples based on the rate constants is OBC > OIC > OIS > OC > OS > OBS. This indicates that OBC adsorbed phosphorus at a rate twice as fast as OS and nine times faster than OBS. Lastly, the pseudo-first-order, pseudo-second-order, and Elovich chemisorption kinetic models were also utilized to analyze data for a 500 mg/L phosphate concentration.

Models	Parameters	Owu Isin Soils	Owu Isin Concretions	Obbo-Ile Soils	Obbo-Ile Concretions	Osi Soils	Osi Concretions
Pseudo first order	$Q_{e(expt)}$ *(mg/g)*	66.80	68.07	67.19	66.42	67.21	67.28
	$Q_{e(model)}$ *(mg/g*	68.08	69.71	69.21	68.10	65.16	68.51
	kF (min^{-1})	0.01085	0.01037	0.01001	0.009740	0.001660	0.01176
	R^2	0.9249	0.9326	0.9268	0.9302	0.9019	0.9099
	SD	5.569	5.45	5.960	5.706	4.466	6.025
Pseudo second order	*Qe (model) (mg/g)*	86.53	89.43	91.64	88.53	76.31	85.64
	kS (g/mg min)	1.250×10^{-4}	1.130×10^{-4}	9.550×10^{-5}	1.040×10^{-4}	2.750×10^{-4}	1.420×10^{-4}
	R^2	0.9983	0.9931	0.9990	0.9991	0.9869	0.9972
	SD	0.5824	1.094	0.4238	0.4489	1.236	0.7362
Elovich chemisorption	*β (g/mg)*	1.883	1.765	1.606	1.630	4.236	2.141
	α (mg/g min)	0.05032	0.04769	0.04687	0.04866	0.06639	0.05162
	R^2	0.9921	0.9859	0.9053	0.9943	0.9747	0.9899
	SD	1.126	1.564	6.778	0.9882	1.527	1.236

Table 3: Kinetic parameter of the adsorption of phosphate onto soils and concretions at 300 mg/L of phosphate

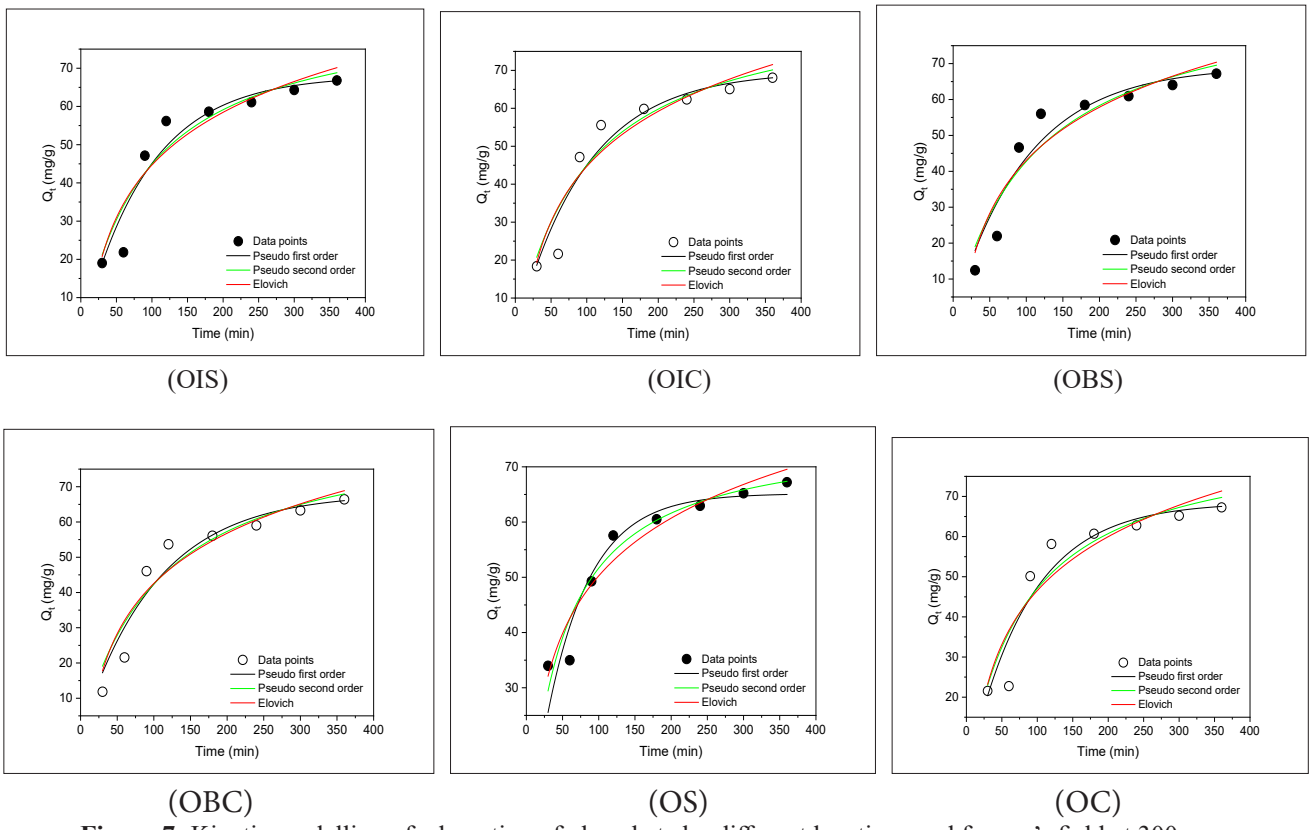

Figure 7: Kinetic modelling of adsorption of phosphate by different locations and farmer's field at 300 ppm

In Table 4 you can find the kinetic profiles of OIS, OIC, OBS, OBC, OS, and OC, as well as a summary of the parameters from the kinetic study. These profiles are also represented graphically in figure 8. The standard deviation (SD) values in the table reveal that the pseudo-second-order model provides the best fit for describing phosphorus adsorption onto all soil samples, surpassing the other two models. The pseudo-second-order model yielded higher R2 values and lower SD values compared to the pseudo-first-order and Elovich chemisorption models. Furthermore, the pseudo-second-order equilibrium adsorption capacities (Qe (model)) for all soil samples were more accurate than the pseudo-first-order predictions in terms of Qe (expt). The rate constants for OIS, OIC, OBS, OBC, OS, and OC are 1.240×10^{-4}, 1.090×10^{-4}, 1.020×10^{-5}, 1.100×10^{-4}, 2.730×10^{-4}, and 1.180×10^{-4} g mg^{-1} min^{-1}, respectively, in ascending order. Based on these rate constants, the phosphorus adsorption rate decreases in the following sequence: OBS > OIC > OBC > OIS > OC > OS. The phosphorus adsorption rate for OBS was twice that of OS, meaning OBS adsorbed phosphorus at twice the rate of OS.

Models	Parameters	Owu Isin Soils	Owu Isin Concretions	Obbo-Ile Soils	Obbo-Ile Concretions	Osi Soils	Osi Concretions
Pseudo first order	$Q_{e(expt)}$ *(mg/g)*	81.93	82.7	82.45	81.89	82.15	83.63
	$Q_{e(model)}$ *(mg/g*	85.82	87.30	87.43	5.572	82.37	87.32
	kF (min^{-1})	0.01235	0.01161	0.01117	0.002240	0.01890	0.01214
	R^2	0.9146	0.9144	0.9072	0.9127	0.9061	0.9266
	SD	7.176	7.511	7.968	7.484	5.267	6.614
Pseudo second order	*Qe(model) (mg/g)*	106.2	109.4	110.4	108.3	94.44	108.4
	kS (g/mg min)	1.240×10^{-4}	1.090×10^{-4}	1.020×10^{-4}	1.100×10^{-4}	2.730×10^{-4}	1.180×10^{-4}
	R^2	0.9962	0.9974	0.9979	0.9974	0.9812	0.9966
	SD	1.042	0.9063	0.8153	0.89626	1.69108	1.018
Elovich chemisorption	*β (g/mg)*	2.910	2.673	2.525	2.644	8.030	2.876
	α (mg/g min)	0.04213	0.04028	0.03962	0.04069	0.05819	0.04108
	R^2	0.9884	0.9903	0.9914	0.9903	0.9658	0.9890
	SD	1.625	1.554	1.495	1.538	2.031	1.626

Table 4: Kinetic parameter of the adsorption of phosphate onto soils and concretions at 500 mg/L of phosphate

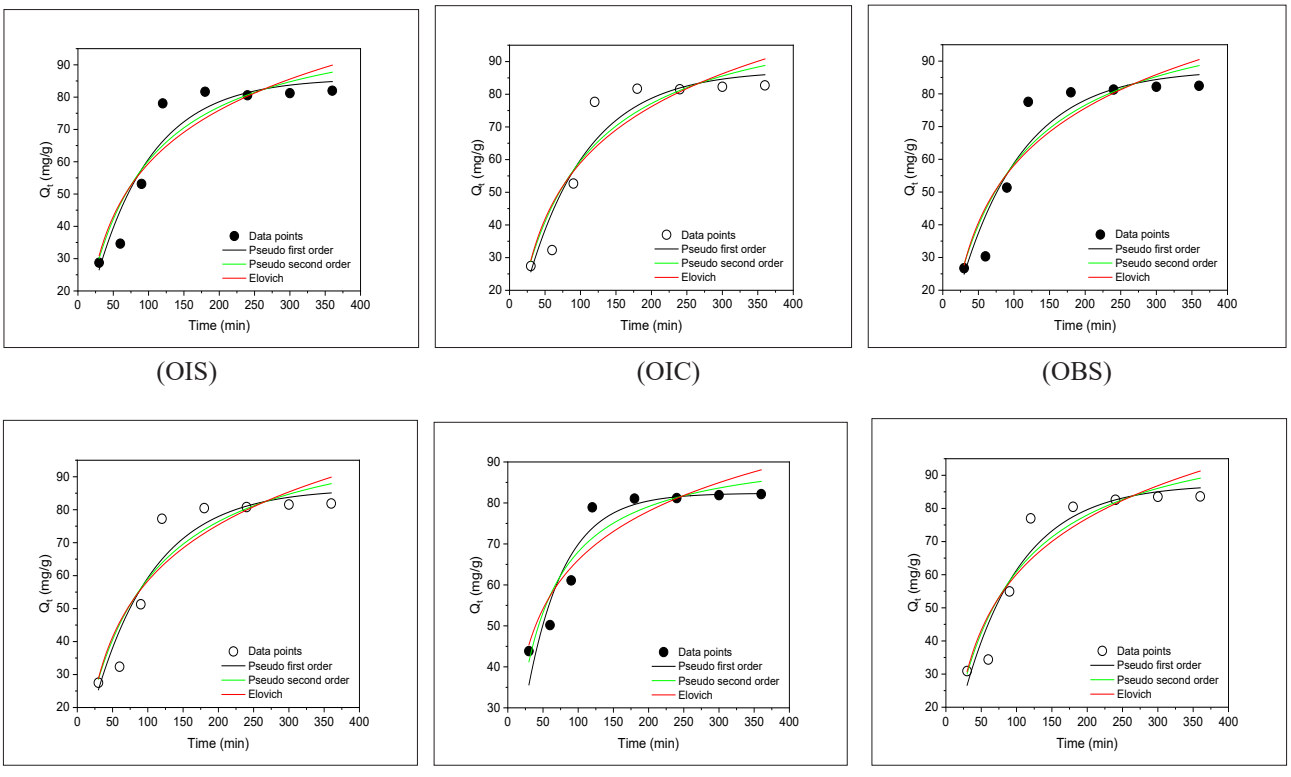

(OIS) (OIC) (OBS)

(OBC) (OS) (OC)

Figure 8: Kinetic modelling of adsorption of phosphate by different locations and farmer's field at 500 ppm

DISCUSSION

Adsorption Isotherm and Kinetics of Phosphorus

Soil and concretions' absorption of phosphates has raised new concerns, affecting agriculture and the environment significantly. Phosphorus, an essential nutrient for plant growth and development, is crucially important for agricultural soils. The release and absorption kinetics of phosphorus play a vital role in managing and monitoring environmental pollution (Agbenin, & Raij, 2001). High phosphorus (P) levels in fluvial water, as transported by rain and domestic and industrial sewers when released into surface bodies like lakes and rivers can cause pollution (Triantafyllidis et al., 2010). Consequently, excess P discharge can lead to serious environmental problems such as eutrophication (Carvalho et al., 2011). Moreover, a comprehensive analysis of phosphorus release and absorption kinetics will reveal detailed insights into the dynamic interactions between phosphorus and soil structure (Hansen & Strawn, 2003). This analysis also aids in quantifying the movement of phosphorus between the solid soil and solution phases. The preferential absorption of phosphate by active soil surfaces converts it into a form that is less accessible and unsuitable for plant uptake (Gonzalez-Rodriguez &

Fernandez-Marcos, 2018). Consequently, phosphorus (P) applied to soil from fertilizer may become unavailable due to fixation and occlusion by iron-enriched concretions (Abdu & Emmanue, 2017). The soil's phosphate adsorption capacity is a key factor in regulating phosphorus levels in the soil solution and determining its availability for plant uptake.

Hence, it is essential to understand how phosphorus is absorbed and released in soils to assess the efficacy of phosphorus fertilizers. Several kinetic equations have been utilized to characterize the kinetics of phosphorus (P) adsorption, such as zero-order, first-order, second-order, and third-order equations, as well as the parabolic diffusion law proposed by (Nafiu, 2009; Agbenin & van Raij, 2001; Nafiu & Raji, 2008; Jalali & Ahmadi Mohammad Zinli, 2011; Jalali & Ranjbar, 2011). Furthermore, the Langmuir equation and the Elovich equation were applied in this context (Hansen & Strawn, 2003). The Langmuir equation assumes that the surface's attraction for the adsorbate remains consistent during the adsorption process. As phosphate (and other specifically adsorbed anions) are adsorbed, the negative charge of the adsorbing surface increases, thereby hindering the adsorption of additional phosphate ions. Consequently, the Langmuir equation is suitable only for low solution ion concentrations, as indicated by Goldberg (Goldberg, 2005). Conversely, at low solution concentrations, the Freundlich equation effectively describes adsorption, assuming that the surface's attraction for the adsorbate diminishes exponentially as adsorption progresses, as mentioned by Goldberg (Goldberg, 2005).

The high level of phosphate sorption, particularly in the OBC as shown in Table 1, suggests that phosphorus will mainly be held in a form that is not readily available, although this varied based on the concentration and location. Gaining a deeper understanding of the physiological mechanisms of phosphorus (P) uptake by roots and foliage, its impact on photosynthesis, its translocation to grains, the synthesis of plant metabolites, and its interaction with other nutrients will offer valuable insights. This knowledge can aid in developing alternative and more efficient fertilizer products and application technologies to optimally meet the biotic needs of P (Noack et al., 2010; Pandey et al., 2013). Organic compounds like humic and fulvic acids, as well as low molecular weight organic acids, vie with phosphate for adsorption sites (Antelo et al., 2007). More so, the presence of organic substances can lead to a notable decrease in phosphate adsorption. Therefore, optimal management of organic matter and crop residues in phosphate-adsorbing soils can significantly increase the availability of phosphorus (Zhu et al., 2018). Furthermore, both soil and concretions exhibit high levels of desorption, indicating a significant risk of phosphorus leaching.

Conclusion

In summary, this research has offered valuable insights into how concretionary nodules affect phosphorus sorption and the characteristics of low-activity clay soils in the Southern Guinea Savannah of Nigeria. Phosphorus (P) sorption in concretions and soil, along with the chemical composition and availability of P in soil and its absorption by plants, are impacted by a complex interplay of physical, chemical, and biological elements, as well as environmental circumstances. The development and distribution of concretionary nodules in savannah soils; are shaped by a variety of factors, including climate, geology, and soil management practices. Nodule formation is significantly influenced by the alternating wet and dry seasons and the addition of iron. Nodules may be absent in the lower soil layers because the consistent moisture inhibits iron dehydration and crystallization.

The study calculated different parameters related to the adsorption of phosphorus (P), such as the maximum phosphorus adsorption (b), affinity constant (k), pseudo-second-order rate constants, and the amount of P adsorbed at the equilibrium solution. The adsorption isotherm demonstrated varying abilities to adsorb phosphorus across different soil types, with the order being OBC > OBS > OIS > OS > OC > OIC. The maximum monolayer adsorption capacities (Qmax values) were 161.0, 154.5, 149.6, 141.7, 139.8, and 139.3 mg/g for OBC, OBS, OC, OIS, OS, and OIC, respectively. The maximum monolayer adsorption capacities (Qmax values) were 161.0, 154.5, 149.6, 141.7, 139.8, and 139.3 mg/g for OBC, OBS, OC, OIS, OS, and OIC, respectively. For P sorbed at 50-ppm equilibrium solution, the pseudo-second-order rate constants were 1.180×10^{-4}, 9.740×10^{-5}, 1.120×10^{-4}, 1.140×10^{-4}, 1.000×10^{-4}, and 8.010×10^{-5} g mg^{-1} min^{-1} for OIS, OIC, OBS, OBC, OS, and OC, respectively. At 300-ppm equilibrium solution, the pseudo-second-order rate constants were 1.250×10^{-4}, 1.130×10^{-4}, 9.550×10^{-5}, 1.040×10^{-4}, 2.750×10^{-4}, and 1.420×10^{-4} g mg^{-1} min^{-1} for OIS, OIC, OBS, OBC, OS, and OC, respectively. Lastly, at 500-ppm equilibrium, the pseudo-second-order rate constants were 1.240×10^{-4}, 1.090×10^{-4}, 1.020×10^{-5}, 1.100×10^{-4}, 2.730×10^{-4}, and 1.180×10^{-4} g mg–1 min^{-1} for OIS, OIC, OBS, OBC, OS, and OC, respectively.

It is understood that the ability of soil to adsorb increases as the pseudo-second-order rate constants increase. According to the study, optimal plant growth in OS soil would necessitate higher P fertilization rates at 50 ppm, while OBC and OBS would require rates of 300 ppm and 500 ppm, respectively, compared to other soils and concretions. Utilizing organic matter and liming in management practices could be advantageous for enhancing crop production in these soils by reducing P adsorption. However, despite recent advancements, there are still significant gaps in our understanding of P sorption influenced by concretionary nodules. The lack of focus on understanding phosphorus retention mechanisms, especially the role of concretions and nodules in phosphorus retention and availability, has created an unresolved paradox in many savannah soils, highlighting the need for further research. Therefore, it is crucial to comprehend the impact of concretionary nodules and low-activity clays on savannah soils for the sustainable management of land in these areas. Taking these factors into account can help optimize agricultural practices to enhance soil fertility, crop productivity, and environmental sustainability in savannah regions. As such,

additional research is necessary to investigate the specific mechanisms by which concretionary nodules and low-activity clays interact with savannah soils and their long-term effects on soil health and ecosystem dynamics.

Reference

1. Abdu, N., & Emmanuel, D. (2017). Soil phosphorus fractions as influenced by concretionary nodules in non-responsive soil in the Nigerian savanna. *Zaria Geographer 24*(1). https://www.researchgate.net/publication/322398648_Soil_Phosphorus_Fractions_as_Influenced_by_Concretionary_Nodules_in_non-responsive_Soil_in_the_Nigerian_Savanna
2. Johan, P. D., Ahmed, O. H., Omar, L., & Hasbullah, N. A. (2021). Phosphorus transformation in soils following co-application of charcoal and wood ash. *Agronomy, 11*(10), 2010. DOI: https://doi.org/10.3390/agronomy11102010
3. Asomaning, S. K., Abekoe, M. K., & Dowuona, G. N. N. (2018). Phosphorus sorption capacity in relation to soil properties in profiles of sandy soils of the Keta sandspit in Ghana. *West African Journal of Applied Ecology, 26*(1), 49-60. https://repository.globethics.net/handle/20.500.12424/25144?show=full&locale-attribute=es
4. Sposito, G. (2008). The chemistry of soils. (2nd Edition) Oxford University Press. https://www.scirp.org/reference/referencespapers?referenceid=1298223
5. Fink, J. R., Inda, A. V., Tiecher, T., & Barrón, V. (2016). Iron oxides and organic matter on soil phosphorus availability. *Ciência e Agrotecnologia, 40*(4), 369–379. DOI:http://dx.doi.org/10.1590/1413-70542016404023016
6. Cordell, D., Drangert, J. O., & White, S. (2009). The story of phosphorus: global food security and food for thought. *Global environmental change, 19*(2), 292-305. DOI: https://doi.org/10.1016/j.gloenvcha.2008.10.009
7. Nafiu, A. (2009). Effects of soil properties on the kinetics of desorption of phosphate from alfisols by anion-exchange resins. *Journal of Plant Nutrition and Soil Science, 172*(1), 101-107. DOI: http://dx.doi.org/10.1002/jpln.200625226
8. Samadi, A. (2006). Phosphorus sorption characteristics in relation to soil properties in some calcareous soils of Western Azarbaijan province. *Journal Agricultural Science Technology*. 8, 251-264. https://jast.modares.ac.ir/article-23-2780-en.pdf
9. de Campos, M., Antonangelo, J. A., & Alleoni, L. R. F. (2016). Phosphorus sorption index in humid tropical soils. *Soil and Tillage Research*, 156, 110-118. DOI: http://dx.doi.org/10.1016/j.still.2015.09.020
10. Hooda, P. S., Rendell, A. R., Edwards, A. C., Withers, P. J. A., Aitken, M. N., & Truesdale, V. W. (2000). *Relating soil phosphorus indices to potential phosphorus release to water, 29*(4), 1166-1171. American Society of Agronomy, Crop Science Society of America, and Soil Science Society of America. DOI: https://doi.org/10.2134/jeq2000.00472425002900040018x
11. Moody, P. W. (2011). Environmental risk indicators for soil phosphorus status. *Soil Research, 49*(3), 247-252. DOI: https://www.publish.csiro.au/sr/sr10140
12. Abdu, N., & Etiene, U. A. (2015). Fifteen-year fallow altered the dynamics of soil phosphorus and cationic balance of a savannah Alfisol. *Archives of Agronomy and Soil Science, 61*(5), 645-656. DOI: https://doi.org/10.1080/03650340.2014.944170
13. Agbenin, J. O. (2003). Extractable iron and aluminum effects on phosphate sorption in a savanna alfisol. *Soil Science Society of America Journal, 67*(2), 589-595. DOI: https://doi.org/10.2136/sssaj2003.5890
14. Zhang, G. Y., He, J. Z., Liu, F., & Zhang, L. M. (2014). Iron-manganese nodules harbor lower bacterial diversity and greater proportions of proteobacteria compared to bulk soils in four locations spanning from north to south China. *Geomicrobiology Journal, 31*(7), 562-577. DOI: http://dx.doi.org/10.1080/01490451.2013.854428
15. Wang, X., Liu, F., Tan, W., Li, W., Feng, X., & Sparks, D. L. (2013). Characteristics of phosphate adsorption-desorption onto ferrihydrite: comparison with well-crystalline Fe (hydr) oxides. *Soil Science, 178*(1), 1-11. DOI: 10.1097/SS.0b013e31828683f8
16. Bortoluzzi, E. C., Pérez, C. A., Ardisson, J. D., Tiecher, T., & Caner, L. (2015). Occurrence of iron and aluminum sesquioxides and their implications for the P sorption in subtropical soils. *Applied Clay Science*, 104, 196-204. DOI: http://dx.doi.org/10.1016/j.clay.2014.11.032
17. Oriola, E. O., Babatunde, O. R., & Salami, A. A. (2019). Soil Characteristics of Cassava Growing Ferralsols and Ferruginous Soils in Kwara State, Nigeria. http://repository.rjt.ac.lk/handle/123456789/4993
18. FAO, (1988). FAO-Unesco Soil Map of the World, Revised Legend. World Soil Resources Report 60. FAO, Rome.
19. USDA, (1975). Soil Taxonomy, a basic system for soil classification for making and interpreting soil surveys. Agricultural Handbook No. 436. USDA, Washington. https://www.scirp.org/reference/referencespapers?referenceid=1559095
20. Murphy, J. A. M. E. S., & Riley, J. P. (1962). A modified single solution method for the determination of phosphate in natural waters. *Analytica chimica acta*, 27, 31-36. DOI: https://doi.org/10.1016/S0003-2670(00)88444-5
21. Excel (2007). Microsoft Word 2007, Microsoft Inc.
22. Agbenin, J. O., & van Raij, B. (2001). Kinetics and energetics of phosphate release from tropical soils determined by mixed ion-exchange resins. *Soil Science Society of America Journal, 65*(4), 1108-1114. DOI: https://doi.org/10.2136/sssaj2001.6541108x
23. Triantafyllidis, K. S., Peleka, E. N., Komvokis, V. G., & Mavros, P. P. (2010). Iron-modified hydrotalcite-like materials as highly efficient phosphate sorbents. *Journal of colloid and interface science, 342*(2), 427-436. DOI: http://dx.doi.org/10.1016/j.jcis.2009.10.063
24. Carvalho, W. S., Martins, D. F., Gomes, F. R., Leite, I. R., da Silva, L. G., Ruggiero, R., & Richter, E. M. (2011). Phosphate adsorption on chemically modified sugarcane bagasse fibres. *Biomass and bioenergy, 35*(9), 3913-3919. DOI: http://dx.doi.org/10.1016/j.biombioe.2011.06.014

25. Hansen, J. C., & Strawn, D. G. (2003). Kinetics of phosphorus release from manure-amended alkaline soil. *Soil science, 168*(12), 869-879. https://www.cabidigitallibrary.org/doi/full/10.5555/20043008954
26. Gonzalez-Rodriguez, S., & Fernandez-Marcos, M. L. (2018). Phosphate sorption and desorption by two contrasting volcanic soils of equatorial Africa. PeerJ, 6, 5820. DOI: https://doi.org/10.7717%2Fpeerj.5820
27. Nafiu, A., Agbenin, J. O., & Raji, B. A. (2008). Kinetic desorption of native phosphorus from soils of varying lithogenic origins in the Nigerian savanna. *Soil science, 173*(12), 837-844. DOI: http://dx.doi.org/10.1097/SS.0b013e31818dacbc
28. Adnan, A. A., Jibrin, J. M., Kamara, A. Y., Abdulrahman, B. L., Shaibu, A. S., & Garba, I. I. (2017). CERES–maize model for determining the optimum planting dates of early maturing maize varieties in Northern Nigeria. *Frontiers in plant science*, 8, 1118. DOI: https://doi.org/10.3389%2Ffpls.2017.01118
29. Jalali, M., & Ahmadi Mohammad Zinli, N. (2011). Kinetics of phosphorus release from calcareous soils under different land use in Iran. *Journal of Plant Nutrition and Soil Science, 174*(1), 38-46. DOI: https://ui.adsabs.harvard.edu/link_gateway/2011JPNSS.174...38J/doi:10.1002/jpln.200900108
30. Jalali, M., & Ranjbar, F. (2011). Effect of addition of organic residues on phosphorus release kinetics in some calcareous soils of western Iran. *Environmental Earth Sciences*, 62, 1143-1150. DOI: http://dx.doi.org/10.1007/s12665-010-0603-6
31. Goldberg, S. (2005). Equations and models describing adsorption processes in soils. *Chemical processes in soils*, 8, 489-517. https://www.scirp.org/reference/referencespapers?referenceid=1893806
32. Noack, S. R., McBeath, T. M., McLaughlin, M. J. (2010). Potential for foliar phosphorus fertilization of dryland cereal crops: a review. *Crop Pasture Sci, 61*(8), 659–669. DOI: https://doi.org/10.1071/CP10080
33. Pandey, R., Krishnapriya, V., & Bindraban, P. S. (2013). Biochemical nutrient pathways in plants applied as foliar spray: phosphorus and iron. VFRC Report, 1, 6-60. https://api.hub.ifdc.org/server/api/core/bitstreams/6b28b846-c80a-44a7-907c-203f723a4459/content
34. Antelo, J., Arce, F., Avena, M., Fiol, S., López, R., & Macías, F. (2007). Adsorption of a soil humic acid at the surface of goethite and its competitive interaction with phosphate. *Geoderma, 138*(1-2), 12-19. https://ri.conicet.gov.ar/bitstream/handle/11336/95033/CONICET_Digital_Nro.163562aa-8b1e-4f08-9b77-65cbc127ee60_A.pdf?sequence=2&isAllowed=y
35. Zhu, J., Li, M., & Whelan, M. (2018). Phosphorus activators contribute to legacy phosphorus availability in agricultural soils: A review. *Science of the Total Environment, 612*(15), 522-537. https://www.sciencedirect.com/science/article/abs/pii/S0048969717320934.